Amyloidogenesis of proteolytic fragments of human elastin†

Brigida Bochicchio,*[a] Antonietta Pepe,[a] Florian Delaunay,[ab] Marina Lorusso,[a] Stephanie Baud[cd] and Manuel Dauchez[cd]

Some polypeptides encoded by the C-terminal region of human tropoelastin gene have been demonstrated to be amyloidogenic *in vitro*. The biological relevance of this finding is still under investigation given that only limited evidence concerning the involvement of elastin in amyloidosis exists. Recent studies identified, by mass spectrometry, several elastin fragments produced from the cleavages made by some elastases in human elastin substrate. Some of these fragments are contained into the same polypeptide sequences previously demonstrated to be amyloidogenic. Our hypothesis is that the up-regulation of elastases in inflammatory processes triggered, for example, by aging induces the release of elastin fragments potentially amyloidogenic. Therefore our aim in this study is to demonstrate if any of these fragments is amyloidogenic *in vitro*. At molecular level, CD, NMR, FTIR spectroscopies and MD simulations were used, while, at supramolecular level, Congo red binding assay and ThT fluorescence spectroscopy complemented with AFM microscopy were carried out. Our results show that the longest peptide, among those synthesized and mimicking the elastin fragments produced by elastases on human elastin, constituted of 22 residues, is able to aggregate into amyloid-like fibres. These findings support the hypothesis of amyloidogenesis of proteolytic fragments of elastin.

DOI: 10.1039/c3ra41893f

Introduction

Elastin is the protein polymer responsible for elasticity in organs and tissues such as lungs, skin and arterial walls.[1–3] Tropoelastin, the soluble precursor of elastin, self-organizes into fibres in the extracellular matrix forming a large, highly cross-linked polymer by interacting with a number of other extracellular matrix proteins. In most tissues elastin production begins around the time of mid-gestation and peaks near birth and during the early neonatal period, then drops dramatically and is nearly completely repressed at maturity. Elastin turn-over is almost absent in normal physiological conditions.[4] Therefore elastin is considered a long-lasting protein that remains for life. However, elastin degradation by enzymes up-regulated during pathological processes has been observed.[5] The degradation of elastin by elastases produces not only a loss in elasticity of the involved tissue, but leads also to the generation of elastin fragments that are often biologically active. For example, elastin fragments are involved in matrix remodelling and exhibit potent chemotactic activity for leukocytes, stimulate fibroblast and smooth muscle cell proliferation, and display pro-angiogenic activity as potent as VEGF.[6] Matrix metalloproteinases (MMPs) are members of a family of enzymes capable of degrading extracellular proteins and comprise MMP-12 that is particularly active against elastin. High concentrations of MMP-12 are found in tissues affected by pathologies such as chronic obstructive pulmonary disease, abdominal aortic aneurysms[7,8] and atherosclerosis.[9] The abnormal levels of MMPs are also associated with skin disorders including granulomatous skin disorders and photoaging where MMP-12 plays an important role.[10] Photodamaged skin leads to qualitative and quantitative alterations of elastin with massive deposition of material, referred to ''elastotic material''. This material is also observed in arteries of atherosclerotic patients[11] and in lung alveoli where the elastotic material was shown to contain amyloid-like fibers.[12] Amyloid deposits were also identified in the vertebral arterial wall of old subjects as they reacted only with a polyclonal antibody to human elastin suggesting this amyloid derived from elastin.[13] This finding could be considered as the first *ex vivo* evidence for the possible involvement of elastin in amyloidogenesis. Before this study, the involvement of elastin in amyloidogenic processes was suggested only by *in vitro*

[a]*Department of Science, University of Basilicata-Via Ateneo Lucano, 10-85100-Potenza, Italy. E-mail: brigida.bochicchio@unibas.it; Fax: (+39)-0971-205678*
[b]*Institut Carnot, CIRIMAT UMR CNRS 5085, Université Paul Sabatier, 31062 Toulouse Cedex 4, France*
[c]*Laboratoire SiRMa, FRE CNRS/URCA N° 3481, Université de Reims Champagne-Ardenne, Reims, France-Moulin de la Housse-51687 Reims Cedex 2, France*
[d]*Plateforme de Modélisation Moléculaire Multi-échelle, UFR Sciences Exactes et Naturelles, Université de Reims Champagne-Ardenne, 51687 Reims Cedex 2, France*
† Electronic supplementary information (ESI) available: ROESY spectrum of S4; turbidimetry graphs; ThT fluorescence graphs; Congo red UV spectra; radius of gyration evolution graphs; AFM of S4; NMR assignment tables; FTIR analysis table; P/G composition analysis table. See DOI: 10.1039/c3ra41893f

Table 1 List of the sequences of elastin proteolytic fragments and of the parent proteases. The sequences are compared with the peptides sequences encoded by exon 28, exon 30 and exon 32. The N-terminal (EX30N) and C-terminal portion of EX30 (EX30-18) are also included. Human tropoelastin protein sequence (Swiss Prot. Accession number P15502.)

Peptide	Sequence[a]	Protease	Amyloidogenic behaviour
S1	^{717}LGVPGVGG^{724}	MMP-12	No
S2	^{709}*LGGLGVGGLG*VPGVGG^{724}	MMP-12	No
S3	^{706}AAG*LGGLGVGGLG*VPGVGG^{724}	Pepsin	No
S4	^{703}LV*GAA*G*LGGLGVGGLG*VPGVGG^{724}	MMP-12	Yes
EX30[12]	^{702}GLV*GAA*G*LGGLGVGGLG*VPGVGGLG^{726}	—	Yes
EX30N[38]	^{702}GLV*GAA*G*LGGLGVGGLG*^{718}	—	Yes
EX30-18[45]	^{709}*LGGLGVGGLG*VPGVGGLG^{726}	—	No
EX32[13]	^{740}*GAA*GLGGV*LGGAG*QFPLG^{757}	—	Yes
EX28[11]	^{657}*GAA*VPGV*LGGLGALGGVG*IPGGVV^{681}	—	Yes
Prion Peptide[46]	A*GAA*AAGA	—	Yes

[a] italic: XGGZG motif; underlined: GAA motif.

studies carried out on the polypeptide sequences encoded by exon 28 (EX28),[14] 30 (EX30)[15] and 32 (EX32)[16] of the human tropoelastin gene (HTE) which were demonstrated to be able to give rise to amyloid-like fibres.[14–16] Recent studies carried out by the Schmelzer group identified the elastin-derived peptides present in an elastase digest of insoluble human skin elastin.[17] Interestingly, polypeptide sequences encoded by exons 28–31 were demonstrated to be present in the elastin lysate. Given these findings and in order to address the biological and pathological results of *in vitro* studies, we hypothesise that elastin-derived soluble peptides released from elastin by proteolytic degradation might slowly aggregate into amyloid-like structures that could explain the amyloid ''elastotic material'' described in numerous reports. In the present work, we chemically synthesised four peptides (S1–S4) that have been shown to be present in the human skin elastin digests by MMP-12 and pepsin[10] and that are present in EX30 sequence (Table 1). Our aim was to assess if any of the four peptides was able to give rise to amyloid-like fibres. CD, NMR, FTIR, Thioflavin-T fluorescence spectroscopies, Congo-red UV assay together with light microscopy (OM) and atomic force microscopy (AFM) techniques were used. Results were complemented with molecular dynamics (MD) simulations.

Results

CD spectroscopy

CD spectroscopy is a useful tool able to define the peptide secondary structures. The conformational analysis of S1–S4 peptides was performed in a qualitative way by comparing the respective curves with CD spectra of polypeptides of known secondary structures or adopting a mixture of unknown structures. To detect possible conformational transitions, useful for understanding the complexity of conformer population, the peptides were monitored by CD spectroscopy in aqueous solution at different temperatures (Fig. 1). The CD spectrum of S4 peptide at 0 °C was characterised by a strong negative band at 195 nm and by a small positive band at 215 nm (Fig. 1a). The increase of the temperature to 25, 37, and 60 °C induced a slight reduction of the positive band and a strong reduction of the negative one. The strong negative π–π^* band at 195 nm is usually attributed either to unordered or to the left-handed poly-proline II conformation (PPII). However, its reduction in intensity on increasing the temperature, together with the presence of the, essentially π–π^* band, at 215 nm, are diagnostic of the PPII conformation.[18–21] The loss of the positive band together with the decrease of the negative one, at higher temperatures, suggested the destabilisation of PPII conformation in favour of a more folded conformation. Indeed, the presence of the isodichroic point at 205 nm was indicative of a conformational equilibrium between only two conformations. The CD spectra of S3 peptide in aqueous solution at the indicated temperatures are shown in Fig. 1b. At 0 °C S3 showed a small positive band at 214 nm and a stronger negative one at 195 nm. Although the spectral features indicated the presence of PPII conformation, however, the negative band of S3 peptide was 2-fold reduced in intensity in comparison with that of S4 (Fig. 1a). This finding suggested that PPII conformation was present in minor amount in S3 compared with S4 peptide.

Overall, the CD spectra suggested for S3 the presence of different conformations quickly interconverting among them. Actually, the absence of the isoelliptic point confirmed the presence of complex equilibria among PPII, more stable at 0 °C, unordered and β-turn conformations.[22–25]

The CD spectra of S1 and S2 peptides are shown in Fig. 1c and 1d, respectively. At 0 °C the CD spectra of S1 and S2 peptides were characterised by two negative bands at 195 and 221 nm, respectively. The increase of the temperature induces the reduction of the negative bands. These findings, together with the absence of the positive band at 215 nm, expected for PPII, suggested the presence of unordered and folded conformations.

NMR spectroscopy

The S3 and S4 peptides were analysed by ^{1}H-NMR spectroscopy in H_2O–D_2O (90 : 10, v/v) at 25 °C. Even though several glycine residues (10 : 19 and 11 : 22 for S3 and S4, respectively) were

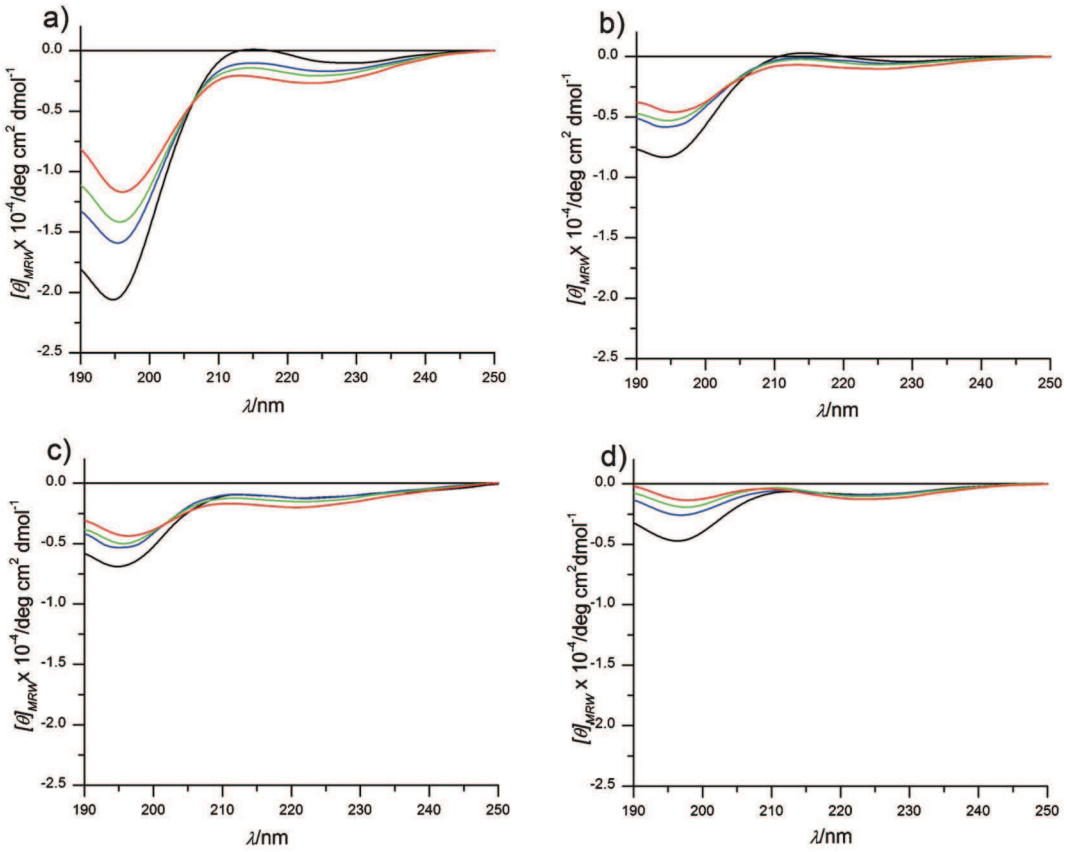

Fig. 1 CD spectra in aqueous solution of: S4 (a), S3 (b), S2 (c), and S1 (d) peptides at 0 °C (black); 25 °C (blue); 37 °C (green); 60 °C (red).

present, complete resonance assignments were achieved for S3 and S4 peptide protons (Supplementary Tables S1 and S2, ESI†, respectively). The ^{1}H-NMR data of both peptides excluded the presence of any folded structures. The chemical shifts of the Hα proton resonances were all in the range usually assigned to unordered conformations.[26] No significant downfield shift was observed, excluding the presence of relevant amount of β-strand at 25 °C. In particular, the glycine Hα protons showed chemical shift values in a very small range, δ 3.88–3.98 ppm, and no differences were observed for the two enantiotopic α-protons. The $^3J_{NH-H\alpha}$ coupling constants of not-glycine residues were in the range 5.8–7.6 Hz, usually assigned to unordered conformations, even though they are compatible also with PPII conformations. Only the valine residues showed higher values, approximately 7.3–8.1 Hz, suggesting a more extended conformation for these β-branched residues. The NH amide proton chemical shifts are those more sensible to environmental condition such as pH, temperature and solvent, while the Hα proton chemical shifts are usually more sensitive to the conformation adopted by the peptide chains. When comparing the amide proton chemical shifts and the Hα proton chemical shifts (Fig. 2) of S3 and S4 peptides, important differences were observed only in the N-terminal regions. These differences were more pronounced for the amide protons. In order to determine the temperature coefficients of the amide protons, 1D spectra were recorded in the temperature range 25–45 °C. For both peptides the temperature coefficients were lower than −5.5 ppb K^{-1}, so excluding the presence of intramolecular H-bonds and of β-turns.[27] While the CD spectra were suggestive of a higher content of PPII conformation in S4 peptide, these NMR data alone were not able to define the presence and relative content of PPII conformation. A careful NOE (Nuclear Overhauser

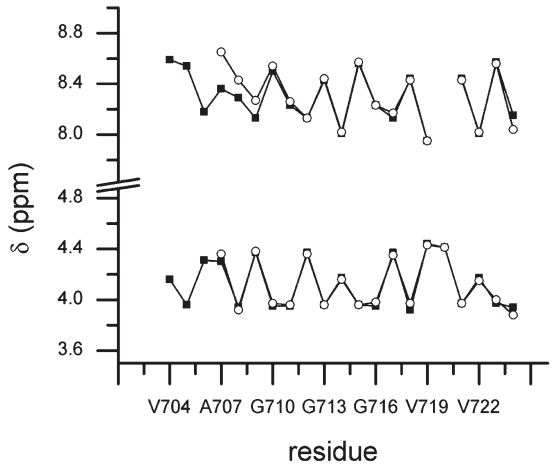

Fig. 2 Comparison of amide proton chemical shifts (top) and Hα proton chemical shifts (bottom) of S3 (circles) and S4 (squares) peptides.

Effect) volume ratio analysis, between sequential $d_{\alpha N}$ and d_{NN} cross-peak volumes was carried out for defining the specific propensities to extended conformations (β-strand and PPII) of the single peptides. As found by Fiebig *et al.*[28] by statistical analysis, the random coil conformation should have a NOE ratio $d_{\alpha N}(i,i+1)/d_{NN}(i,i+1)$ equal to 1.4 for the sequential backbone cross-peaks, while for the extended conformations the higher distance of sequential amide protons should increase the ratio to a value of 55.[29] Fig. S1, ESI† of the Supporting Information shows the fingerprint (NH–Hα) and the amide (NH–NH) regions of the Rotating Frame Overhauser Effect Spectroscopy (ROESY) spectrum of S4 peptide. The regions are displayed with the same threshold in order to highlight differences in intensity of the cross-peaks. From the analysis of NOE volume, we were able to define the NOE volume ratio for some not overlapping peaks of S4 peptide, focusing in particular on the N-terminal region. The ratio values found for G_{705}, A_{707} and L_{709} residues, ranging from 5.54 to 40, were significantly higher than those expected for residues adopting random coil conformations thus suggesting that the time spent in extended conformations (β-strand and/or PPII) by these residues at 25 °C is significant. The same analysis was not possible for the S3 peptide where coincidental chemical shift values did not permit to determine the contribution to the NOE volumes of different proton connectivities. Altogether, the CD and ^{1}H-NMR data of both peptides pointed out the presence of highly flexible, unstructured conformations, populating different secondary structures. In order to define quantitatively the conformational ensemble and to highlight possible differences that could account for the different aggregation propensities observed for S3 and S4 peptides, we measured ^{13}C chemical shifts of the Cα and CO backbone carbons and the Cβ carbons from 2D Heteronuclear Single Quantum Correlation (1*H*-13C HSQC) and Heteronuclear Multi-Bond Connectivity (1*H*-13C HMBC) spectra. The measured chemical shifts of S3 and S4 peptides were submitted to the δ2D method analysis,[30] available online (http://www-vendruscolo.ch.cam.ac.uk/d2D/index.php). The results are shown in Fig. 3. We found that the probability to adopt similar secondary structures from L_{709} to G_{724} in both peptides was very high. Appreciable differences between S3 and S4 peptides were only observed at the N-terminus of S4, where V_{704} and G_{705} showed significant probability to adopt extended (β-sheet and/or PPII) conformations that could trigger the amyloid–like self-assembly propensity observed for S4 peptide.

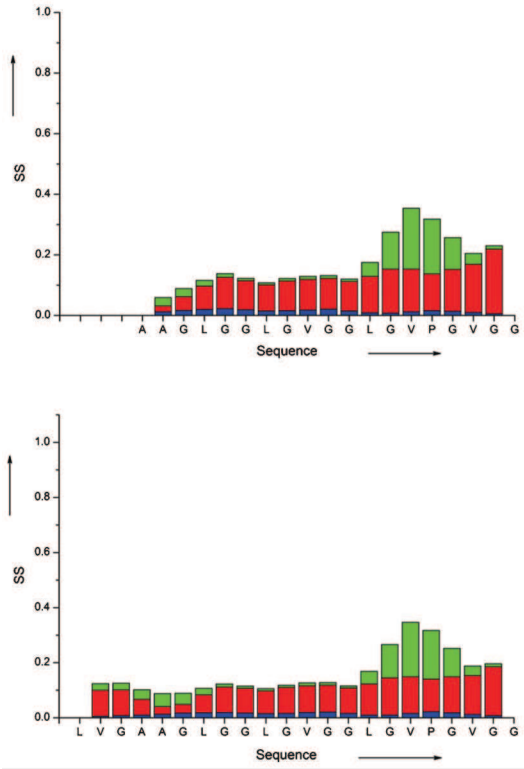

Fig. 3 Secondary structure populations, as obtained using the δ2D method, for S3 (top) and S4 (down) peptides; secondary structures are shown in red (β-sheet), blue (α-helix) and green (PPII).

Turbidimetry experiments

In order to investigate the aggregation properties of the synthesised peptides, measurements of turbidimetry on apparent absorbance (TAA) values were carried out as a function of temperature by turbidimetry. Turbidity measurements showed that, on increasing the temperature, only the S4 peptide solution gave rise to an irreversible TAA value increase due to the aggregation of the peptide at 60 °C (Fig. S2A of supporting information, ESI†). These findings strongly suggest for S4 an irreversible inverse-temperature phase transition compatible with an amyloid-like behaviour. Even if the critical temperature observed for the phase transition is not the physiological one, we argue that it could approach physiological values by changing some variables, such as peptide concentration and time. As shown in Fig. S2B, ESI† of supporting information, S4 peptide is able to self-aggregate in one week at physiological temperature, and it has to be reminded that these and longer times are compatible with physiological/pathological events *in vivo*.

Thioflavin-T fluorescence assay

Thioflavin-T fluorescence assay represents a useful tool to reveal the presence of amyloid-like fibrils. Thioflavin-T (ThT) is a fluorescent dye suggested to bind rather selectively to the β-sheet structures of amyloid-like fibres.[31–33] The addition of ThT to the S4 peptide solution induces an increase of the ThT emission band centred at 482 nm, as expected for amyloid-like fibrils (Fig. S3 in supporting information, ESI†). On the other hand, the addition of the S1, S2 and S3 peptides to the ThT solution does not change the fluorescence spectrum of ThT (data not shown).

Congo red spectral shift assay

Congo red is a diazo dye that is widely used to characterise amyloid-like fibres being its binding specifically dependent on the secondary structure characteristic of the fibrils. It has been demonstrated that the interaction of the Congo red with β-pleated sheet conformation[33,34] induces two effects in the UV spectrum of peptides, the hyper-chromic effect (increase in absorbance) and the bathochromic effect (red shift of

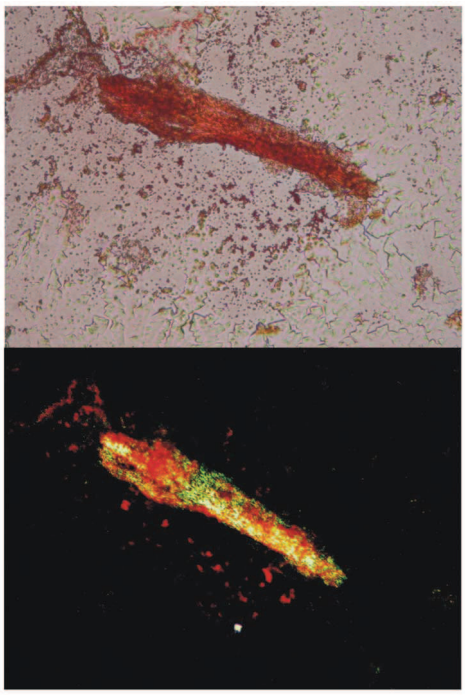

Fig. 4 Optical microscopy images of S4 fibrils stained with Congo red: bright field (top) and dark field (bottom).

maximum absorbance wavelength). The interaction of S4 with Congo red dye induced both the strong hyper-chromic and bathochromic effects (Fig. S4 in supporting information, ESI†). S1, S2 and S3 peptides did not produce hyper-chromic nor bathochromic effects in the UV absorption spectrum (data not shown).

Congo red birefringence assay

It is well known that amyloid plaques extracted from the brain of patients affected by Alzheimers disease exhibit an apple-green birefringence under a dark field in light microscopy.[34,35] This characteristic has been ascribed to an ordered arrangement of the elongated structure within the amyloid fibrils as it is an index of a highly organised sub-structure. An aliquot of each peptide from 'Congo red spectral shift assay' was observed by light microscopy under cross-polarized light. Only S4 peptide exhibited the apple-green birefringence characteristic of amyloid-like fibres (Fig. 4).

FTIR spectroscopy

In FTIR spectroscopy, the amide I, due to the stretching vibrations of the C=O group of the peptide backbone, is the most informative region on protein secondary conformation. Furthermore, amide I is stronger than amide II which originates from the combination of the N–H bending and C=O stretching modes, and than amide A modes which originate from the N–H stretching. In the present study, only the amide I and II modes were analysed. FTIR measurements were carried out on the lyophilised powders of S1–S4 peptide.[31] The decomposed FTIR spectra of the amide I and II regions are shown in Fig. 5 a–e. The results are summarised in Table S3, ESI† of the supporting information which gives the position, the area values and the assignment of the main individual components of the band fits. The decomposed FTIR spectra of the amide I region showed, for all the lyophilised peptides, but S3, a component in the range 1625 and 1634 cm^{-1} that could correspond to the vibrational modes of hydrogen bonded β-turns and/or β-pleated sheets. These components, together with the additional ones observed in the range 1685 and 1697 cm^{-1}, could be assigned to vibrational modes of antiparallel β-sheet conformations compatible with the presence of the cross-β structure.[36,37] The component at 1643 cm^{-1}, observed only for S3, is due to the absorption of water usually found between 1640–1650 cm^{-1}.[38] Each peptide showed in the amide I region the presence of a component in the range between 1661 and 1667 cm^{-1}. The bands comprised in this range are usually assigned to non-hydrogen-bonded C=O groups or groups weakly bonded to the solvent.[39] In our measurements, because of the absence of the solvent, the band is essentially due to the presence of PPII conformation, which is an extended structure lacking intramolecular hydrogen bonds. Finally, the components in the range 1648–1652 cm^{-1} are due to the contribution of unordered conformations. The components of decomposed amide II region comprised in the range 1537–1539 cm^{-1} were tentatively assigned to unordered conformations.[40] The components in the ranges 1517–1521 cm^{-1} and 1552–1558 cm^{-1} could be attributed to antiparallel β-sheets.[41,42] Indeed, the peak at 1521 cm^{-1} for S1 is normally attributed to the dominance of the bending of hydrogen bonded NH groups in antiparallel β-sheet structures.[43] Overall, the FTIR analysis showed for all four peptides, in lyophilised powder, the presence of multiple conformations comprising an ensemble of β-sheet, PPII and unordered conformations. Additionally, FTIR measurements were carried out on S4 aggregates (Fig. 5a) in order to gain useful insights into the secondary structure of S4 fibres (Fig. 5a). Even if the frequencies of amide I band components were very similar to those found for S4 lyophilised powder, the ratio among the areas of each components drastically changes. The total area of the bands assigned to antiparallel β-sheet, centred at about 1630/1697 cm^{-1}, was significantly increased in S4 fibres (Table S3, ESI† of the supporting information). This finding suggested that the cross-β structure was predominant in S4 fibres. The presence of cross-β structure was compatible with the amyloidogenic nature of S4 aggregates. Decomposed amide I region FTIR spectra of S3 and S4 peptides collected in D_2O solution are displayed in Fig. 5f and 5g. For S4 peptide a dominant component at 1672 cm^{-1} assigned to PPII conformation was visible together with two additional minor components at 1650 and 1642 cm^{-1} due to random coil and β-sheet conformation, respectively. Decomposed amide I region FTIR spectrum of S3 showed two components of comparable intensities at 1673 and 1649 cm^{-1} indicative of PPII and random coil conformations, respectively. A minor component was found at 1638 cm^{-1} and assigned to β-sheet conformation. On summarising, the FTIR spectra in D_2O solution confirmed that the PPII conformation was dominant in S4 peptide while the conformational space of S3 peptide was equally populated by PPII and random coil conformers, as also inferred by NMR and CD studies.

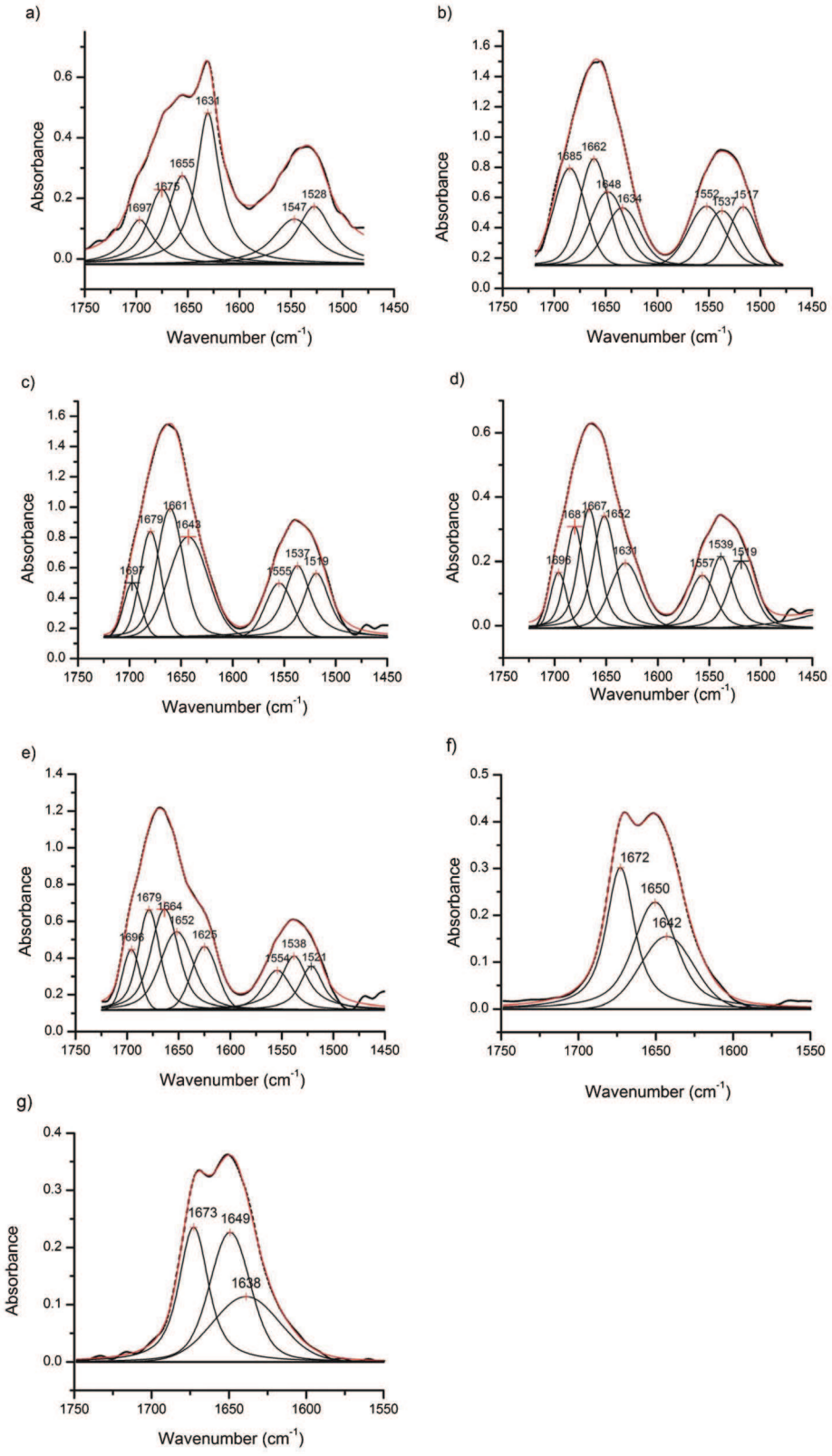

Fig. 5 Decomposed FT-IR spectra of S4 fibres (a) and of S4 (b), S3 (c), S2 (d), S1 (e) lyophilized peptides in KBr pellet. The band fitting results of amide I and II regions are shown. Dashed line: experimental spectrum. Solid line: calculated spectrum. Decomposed FTIR spectra of amide I region in D_2O solution of S4 (f) and S3 (g) lyophilized peptides.

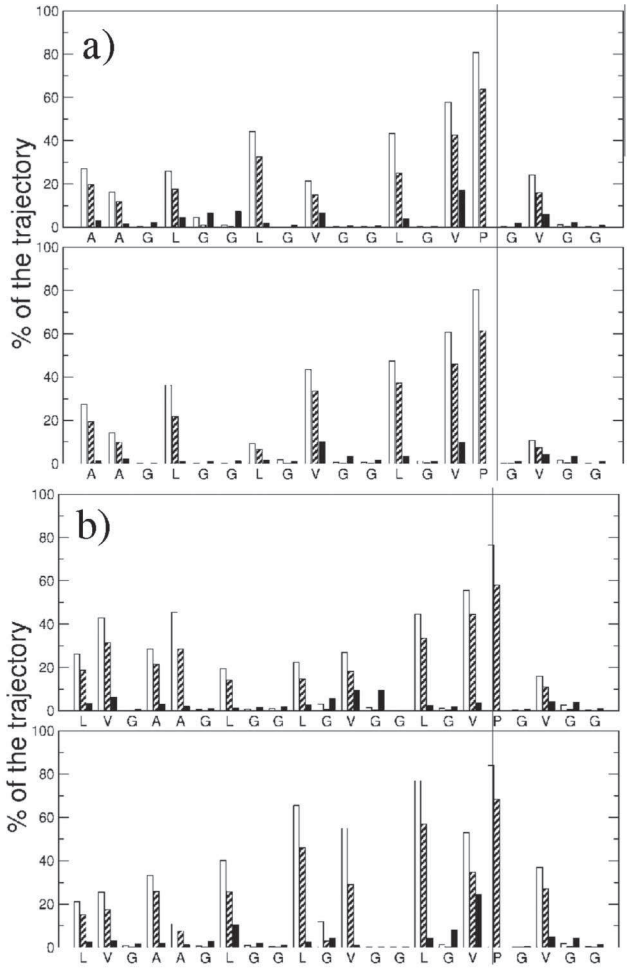

Fig. 6 Secondary structures of S3 (a) and S4 (b) peptides. The secondary structure of the S3 and S4 peptides are evaluated in terms of PPII and β-sheet contents as a percentage of the trajectory. Since these two configurations correspond to similar areas in the Ramachandran plot, the content of β-sheet (full bars) was evaluated considering φ and ψ angles with a deviation of $\pm$ 20° from the canonical values. The content of PPII was evaluated using successively a deviation of $\pm$ 30° (empty bars) and of $\pm$ 22° (dashed bars) from the canonical values. For each peptide, we represent the secondary structure content over the trajectory both for the elongated starting conformation (top panels of (a) and (b)) and the PPII starting conformation (bottom panels of (a) and (b)).

MD simulations

We analysed the two trajectories of S3 and S4 peptides in terms of PPII, β-turns and β-sheet formation and interconversion, as a function of time at the physiological temperature of 37 °C starting from two different conformations *i.e.* PPII and elongated conformation. No significant differences were found at the level of starting conformation. The first analysis was the computation of the radius of gyration of the peptides that gives an idea of their overall folded state. The corresponding results are presented in Fig. S5, ESI† of the supporting information, where the radius of gyration of S3 and S4 was plotted *versus* time. It has been observed that for the two peptides, the radius of gyration decreased rapidly at the beginning of the simulations (within the first 10 ns) and reached stable values around 7 Å, in a manner not dependent on the starting structure. The decrease observed at the beginning of the simulations as well as the low value of this parameter during the simulations, attested the hydrophobicity of the peptides that collapse on themselves in order to optimise self-interactions and interactions with the solvent and to adopt very compact structures. During the visualisation of the trajectories, some transient antiparallel or parallel β-structure could be observed only for S4 peptide at the end of the trajectory (Fig. S5 in supporting information, ESI†). In Fig. 6, data are reported that allowed to characterise the local structure of the peptides during the simulations not only in term of β-structure but also in term of PPII structure. In order to identify the two types of structures, computations of the dihedral angles were performed and a deviation of $\pm$ 30° was tolerated around the canonical values of the (φ, ψ) dihedral angle values [(φ, ψ) = (−75°, + 145°) for the PPII structure and (φ, ψ) = (−119°, + 113°) in the case of parallel β-sheet]. A more stringent deviation of $\pm$ 22° was also used in order to distinguish between PPII and parallel β-sheet, that can be overlapping structures, using a $\pm$ 30° deviation. While the presence of PPII conformation was assessed for both peptides, the percentage of the trajectory populated by PPII was higher for S4 peptide. Limited evidences of significant β-sheet conformation were also observed.

Atomic Force Microscopy

AFM microscopy provides a three-dimensional characterisation of the fibrils and represents a valid tool to investigate the presence of amyloid-like fibrils. The AFM micrographs of the S4 peptide showed a dense network of intertwined fibrils (Fig. 7a). A hierarchical organisation of S4 fibrils has been observed (see arrow in Fig. 7a). In particular, it is evident that the fibrils exhibit regular periodicity. The fibrils are often made by two main filaments interacting side by side or splitting into two thinner filaments. S1, S2 and S3 peptides give rise to an amorphous peptide film (Fig. 7c–e). In particular, Fig. 7c shows that the S3 amorphous peptide film is characterised by circular defects ranging from 25 to 100 nm in diameter. AFM studies definitely confirmed that among the synthesised peptides only S4 was able to give rise to amyloid-like fibrils. The substrate onto which the proteins are deposited plays a tremendous role in dictating the orientation/morphology/behaviour, therefore S4 aggregates were observed on Si as well as on mica substrate (Fig. S6 and S7 of supporting information, ESI†). In both cases, similar intertwined fibrils were observed thus excluding the role of substrate in the morphology of S4 aggregates.

Discussion

The results of this study show that S4 peptide, one of the products obtained from MMP-12 proteolytic cleavage of the human skin elastin, is able to give rise to an aggregation process induced by environmental changes such as temperature and time. The end product of the aggregation consists of fibres with an amyloid-like structure. The criteria adopted to

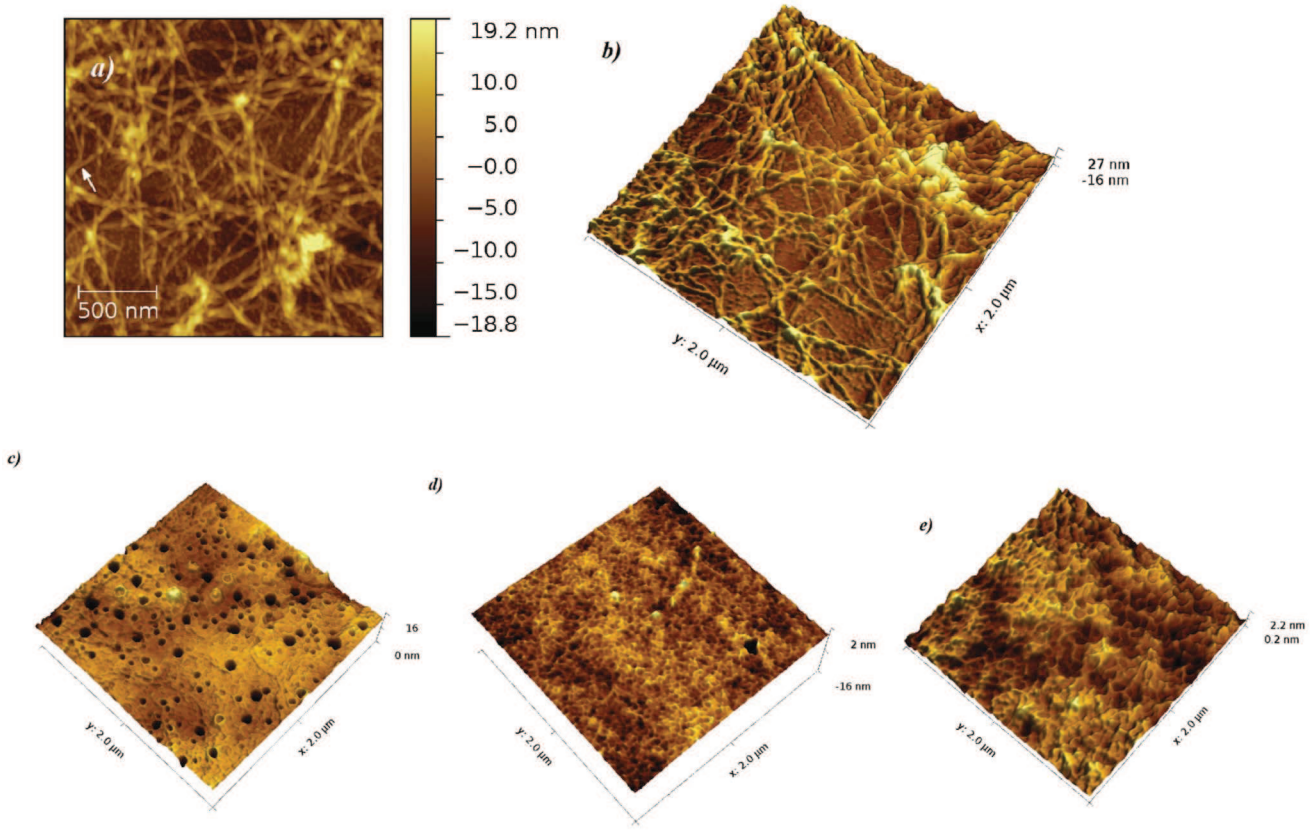

Fig. 7 AFM micrograph of S4 fibres (a); 3D-AFM micrographs of S4 fibers (b), S3 (c), S2 (d), and S1 (e) peptides deposed on silicon wafer and observed in air.

assess the presence of amyloid-like fibres are well known in the literature and are based on a combination of different techniques. In this study, positive results for Congo red binding assay and Congo red birefringence combined with the presence of intertwined fibres, together with the high amount of β-sheet structure at molecular level, assessed by FTIR spectroscopy, are adequate evidences of an amyloid-like aggregating S4.[44]

Concerning the molecular structure in aqueous solution, representing the pre-fibrillar state of the peptide, CD, NMR, and FTIR studies demonstrated that S4 peptide is characterised by the presence of PPII conformation together with a less represented folded conformation. The ratio of the two conformations depends on the temperature, with the PPII structure being preferred at 0 °C.[22] For the remaining S1–S3 peptides, PPII is a minor (S3) or totally absent conformation (S1, S2), even at low temperature. As only S4 peptide gave rise to amyloid-like fibres, a relationship between the molecular and supramolecular structures for peptides has been assessed showing that the PPII conformation is fundamental in order to have amyloid-like structures. Actually, the presence of PPII conformation was ascertained in the pre-fibrillar state (solution state) of many other elastin-derived peptides able to self-assemble into amyloid-like fibres.[14,16] This finding is reinforced by studies inferring the presence of PPII conformation in Aβ(1–28)[45] and Aβ(12–28)[46] amyloidogenic peptides. Therefore, we consider the presence of PPII as an hallmark for the potentially amyloidogenic behaviour of elastin peptides. The presence of β-sheet conformation in the fibrils was investigated by solid state FTIR. Since the molecular studies carried out by CD spectroscopy gave useful insights into the conformations involved in the prefibrillar state of S4 peptide, FTIR let us to investigate the fibrillar state thus providing complementary information. Solid state FTIR also allowed the comparison between the non aggregated (S1–S4) and the aggregated state (S4) of peptides. FTIR analyses evidenced for all peptides a mixture of conformations consisting of PPII, unordered and β-turn conformation together with antiparallel β-sheet that become dominant in S4 fibres, as expected for amyloid-like peptides[47] (Fig. 5, Table S3, ESI† of the supporting information). On this basis, and taking into account the CD, NMR and FTIR data, we suggest that PPII, a flexible structure devoid of intramolecular hydrogen bonds, coexists with β-sheet and could easily interchange into cross-β structure.[48] The conformational transition from PPII to cross-β structure could be responsible for the irreversible precipitation of the soluble peptide into amyloid-like aggregates. Previous studies on elastin-derived amyloidogenic peptides proposed a model of the conformational transition from soluble protofilaments, mainly structured in PPII conformations, to insoluble mature fibres structured in cross-β conformation. The conformational transition from PPII to β-sheet conformation is highly

probable given the similarity of the dihedral angle values of the two conformations located in the upper-left region of the Ramachandran map (φ, ψ) = +180° to 0°. The hypothesis made on the aggregation mechanism involved is that the hydrophobic interactions due to hydrophobic amino acids (A, V, L) are the driving force of the aggregation processes.[49,50] Actually, by increasing the temperature of the peptide the hydrophobic interactions are favoured thus determining the transition to the β-sheet conformation. The possibility that the formation of β-structures gives rise to the aggregation is consistent with the more general mechanism proposed for the formation of amyloid fibres by proteins such as lysozyme and transthyretin where the formation of fibres is consequence of an unfolding process, induced by changes in microenvironment, leading to the formation of fibres and other aggregates that accumulate in the extracellular space.[15]

The role played by the peptide secondary structure in the amyloid-like self-aggregation process is strictly connected to the peptide sequence. Generally, proline-rich elastin-derived peptides self-aggregate upon heating in a reversible process, known as coacervation, as tropoelastin does. The peptide coacervate is constituted by hierarchical fibrous organisation very similar to the supramolecular structure exhibited by the entire protein.[51,52] On the other hand, some glycine-rich elastin-derived peptides, upon heating, give rise to an irreversible self-aggregation process whose final aggregates are, at supramolecular level, intertwined fibres similar to amyloid-like filaments.[53] Among glycine-rich elastin-derived peptides, EX30 containing all the four synthesised peptides S1–S4, was demonstrated to self-aggregate into amyloid-like fibrils.[15] The different behaviour of proline and glycine-rich elastin-derived peptides has been recently rationalised by experimental and Molecular Dynamic studies.[54,55] The analysis is mainly based on the glycine and proline content of the peptides: the hindered proline and the flexible glycine, the most abundant amino acidic residues in elastin, play a crucial role in triggering the self-aggregation properties of elastin-derived peptides.[14,55,56] According to Pomes,[55] the sequence analysis of some elastin sequences shows a threshold in proline and glycine composition above which amyloid formation is impeded and elastomeric properties become apparent. In our case, EX30 peptide reveals a P and G composition consistent with a grey region where both amyloidogenic and elastomeric properties can coexist. By adopting the same analysis we find that the gradual lengthening of the sequence from S1 to S4 reduces the P percentage content thus conferring to the longer peptides a progressive increase of the amyloidogenic properties, according to our experimental data (Table S4, ESI† of the supporting information). In the present work the issue of a better understanding of the sequence-structure relationship for amyloidogenic elastin-derived peptides has been addressed. Indeed, previous studies have demonstrated that the propensity of elastin-derived peptides to aggregate in amyloid-like fibres is dependent on the primary structure of the peptide. Accordingly, the elastin-derived peptides containing the XGGZG (X, Z = V, L, A) motif, tandem or twice repeated, were demonstrated to adopt an amyloid-like structure that was considered responsible for their amyloidogenic behavior.[16] Furthermore, the peptide sequences containing this motif are widely found in many proteins such as collagens IV and XVII, fibrillin 2 precursor, flagelliform silk protein, major ampullate gland dragline silk protein, major prion protein precursor, lamprin precursor, as well as in amyloid AβA4 precursor protein-binding family. Concerning the peptides synthesised in this work, it is worth of note that all the peptide sequences listed in Table 1, but S1 peptide, contain the motif XGGZG (X, Z = V, L, A) tandem repeated along the peptide sequence. However, even if this finding is in good agreement with the amyloidogenic nature of S4, it does not explain the different behaviour of S3 and S2 peptides when compared to S4. S4 differs from S3 only in three additional residues ($L_{703}V_{704}G_{705}$) located at the N-terminus of the sequence. In this way, a G_{705} A_{706} A_{707} triplet is introduced in the longer S4 sequence (Table 1).

Interestingly, the GAA motif is also found in EX28,[14] EX30,[15] EX30N[48] and EX32[16] elastin sequences previously demonstrated to be amyloidogenic, as well as in the highly amyloidogenic AGAAAAGA peptide[57] (Table 1). Therefore, it could be speculated that the GAA motif could be responsible for the major amount of PPII conformation found for S4 in comparison with S3, as inferred by CD studies, and responsible for S4 amyloidogenic behaviour.

In order to support this finding, NMR and MD analyses focused the attention on the N-terminal region. Essentially, NMR and MD results confirm the CD insights suggesting for S4 peptide a higher propensity, in comparison with S3, to adopt the PPII conformation due to A_{706} and A_{707} residues. In particular, by using ^{1}H and ^{13}C chemical shifts of S3 and S4 peptides, an attempt to define quantitatively the different secondary structures populated by the residues was made. The use of chemical shifts for the identification of secondary structures in the native state of globular proteins has been long recognised.[26,58] In the case of disordered or natively unstructured states of proteins and peptides, the quantitative identification of the secondary structures uniquely based on the backbone chemical shifts was a demanding task.[30] Recently, Camilloni *et al.* developed a new method, based on the backbone chemical shifts of disordered states of proteins, that has been applied on several unstructured states of proteins.[30] The δ2D method is very useful to identify the probability of the distribution of heterogeneous secondary structures defining the conformational ensemble populating the proteins. In our case the δ2D method suggests a significant propensity to extended conformations (β-sheet and PPII) for the N-terminal residues of S4 (Fig. 3) and this could account for the increased aggregation propensities observed for S4 peptide.

In order to have additional insights into different aggregation propensity of S3 and S4 peptides, we submitted our sequences to several servers, hosting softwares aimed to predict and/or to identify, inside the peptide sequences, the segments more prone to aggregation. A systematic search,

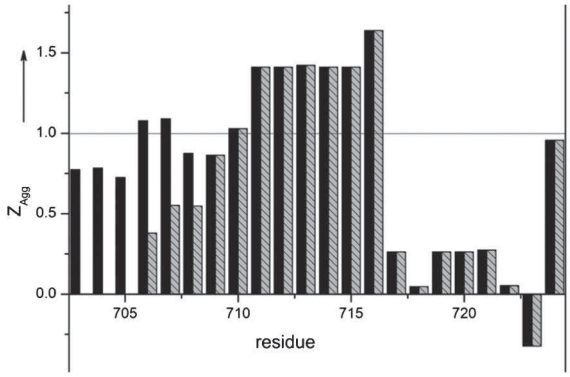

Fig. 8 Aggregation propensity profiles of S3 and S4 sequences. The vertical bars indicate the intrinsic aggregation profile of S3 (gray dashed) and S4 (black) peptides.

employing several available software [BETASCAN,[59] TANGO,[60] AmylPred,[61] FoldAmyloid,[62] AGGRESCAN,[63] WALTZ,[64] Zyggregator[65]] [reviewed in[66]] evidenced similar results. According to AGGRESCAN results, the regions with a higher propensity to adopt β-sheet structures are G_{705}–A_{707} and L_{713}–V_{719} in S4, while in S3 only the latter region was identified as prone to aggregation. Similar results have been achieved by Zyggregator analysis. According to Zyggregator, S4 shows two regions with high aggregation propensities (those above the $Z_{Agg} = 1$ threshold, dotted line in Fig. 8): the N-terminal region A_{706}–A_{707}, absent in the S3 peptide, and the G_{710}–G_{716} regions, present also in the S3 peptide.

Even if the theoretical results are to be considered with great caution, nevertheless they confirm our experimental data suggesting that the N-terminal region of the two peptides have different aggregation propensities that could account for the observed results. Now, we would like to discuss, admittedly in a speculative manner, the possible relevance of these findings to some pathologies that affect elastic tissues and where MMP2 protein and activity were found (*e.g.* atherosclerosis, chronic obstructive pulmonary disease, abdominal aortic aneurysms). Therefore, elastin can potentially release amyloidogenic fragments by up-regulating proteolytic enzymes in pathological conditions and in ageing.

We have shown that elastin proteolytic fragments are potentially able to form amyloid-like aggregates at physiological temperature and times. However, clear clinical evidences that elastin-related amyloids are involved in pathological conditions are lacking. In the arterial wall fragments of various proteins were involved in the age-related amyloid deposition. In particular, medin, a fragment derived from lactadherin expressed by smooth muscle cells, aggregates into amyloid in certain arteries, particularly the thoracic aortic media layer.[67] Immunohistochemical findings showed that medin amyloid co-localizes with elastic fibres in arteries[67] and increases the production of metalloproteinases, thus favouring elastin and collagen degradation.[68]

Conclusion

Elastin self-assembles into fibres and bundles of filaments that are crucial for its biological function and appear as twisted-rope and very different from the amyloid-like fibrils formed by some elastin-derived peptides. In this work we have shown that one peptide, among the four synthesised, is able to give rise to amyloid-like fibrils, *in vitro*, as a function of temperature and time. This finding supports the initial hypothesis well, suggesting that elastin is involved in amyloidogenesis only when elastin-derived peptides are released from the protein, for example by the action of proteases up-regulated in ageing and in pathological processes. Among the assayed peptides, S4 seems to have the highest propensity to produce amyloid-like structures due to the GAA motif responsible for the prevalent PPII conformation of the peptide.

Experimental section

Peptide synthesis and purification

The peptides were synthesised by solid-phase methodology using an automatic synthesiser APPLIED BIOSYSTEM model 431 A. Fmoc/DCC/HOBT chemistry was used, starting from (0.25 mmol) Wang resin (Nova Biochem, Laufelfingen, Switzerland). The Fmoc-amino acids were purchased from Nova Biochem (Laufelfingen, Switzerland) and from Inbios (Pozzuoli, Italy). The cleavage of the peptides from resin was achieved by using an aqueous mixture of 95% trifluoroacetic acid. The peptides were lyophilised and purified by reversed-phase HPLC (high performance liquid chromatography). Binary gradient was used, and the solvents were H_2O (0.1% TFA) and CH_3CN (0.1% TFA). The purity of peptides was assessed by electrospray mass spectrometry.

CD spectroscopy

CD spectra of peptides (0. 1 mg ml^{-1}) were acquired at different temperatures with a Jasco J-815 Spectropolarimeter equipped with a HAAKE thermostat as temperature controller by using 0.1 cm path length quartz cell. Samples were equilibrated at the temperature for 5 min before acquisition. Spectra were acquired by taking points every 0.1 nm, with 100 nm min^{-1} scan rate, 16 scans, an integration time of 2 s, and a 1 nm bandwidth. The data are expressed in terms of $[\theta]_{MRW}$, the mean residue ellipticity value as deg cm^2 $dmol^{-1}$, in order to compare the data obtained for different peptide lengths.

NMR spectroscopy

All NMR experiments were performed on a Varian Unity INOVA 500 MHz spectrometer equipped with a 5 mm triple-resonance probe and *z*-axial gradients. The purified peptides were dissolved in 700 μL H_2O–D_2O (90 : 10, v/v) containing 0.1 mM 3-(trimethyl-sily1)-1-propane sulfonic acid (DSS) as internal reference standard at 0 ppm. 3 mM peptide solutions were used. One-dimensional spectra were acquired in Fourier mode with quadrature detection and the water signal was suppressed by double-pulsed field-gradient spin-echo.[58] Two-

dimensional Total Correlation Spectroscopy (TOCSY[59]) and ROESY[60] spectra were collected in the phase-sensitive mode using the States method. Typical data were 2048 complex data points, 32 or 64 transients and 256 increments. Relaxation delays were set to 2.5 s and spinlock (MLEV-17) mixing time was 80 ms for TOCSY while 200–300 ms mixing time was applied to ROESY experiments. Shifted sine bell squared weighting and zero filling to 2 K × 2 K was applied before Fourier transform. Amide proton temperature coefficients were usually measured from 1D ^{1}H NMR spectra recorded in 5 °C increments from 20 °C to 45 °C. Data were processed with VNMRJ 2.2D. ^{1}H Sequential resonance assignments were made by the approach described by Wüthrich.[61] The 2D ^{1}H–^{13}C gradient heteronuclear single quantum correlation (adiabatic version) (gHSQCAD) and the gradient heteronuclear multi-bond connectivity (adiabatic version) (gHMBCAD) experiments were carried out with the natural abundance of ^{13}C in the S3 and S4 peptides using the pulse sequences from the Varian user library. The ^{13}C resonances were assigned through the 2D ^{1}H–^{13}C HSQC and ^{1}H–^{13}C HMBC spectra by using the assigned ^{1}H chemical shifts for proton resonances.

Turbidimetry experiments

1.5 ml of 1 mM solutions of the synthesised peptides in TBS buffer [Tris (50 mM), NaCl (1.5 M), and $CaCl_2$ (1.0 mM) (pH 7.0)] were analysed by turbidimetry at 440 nm as function of temperature and at 37 °C as a function of time for one week on a Cary 50 UV spectrophotometer equipped with a Peltier temperature controller using quartz cells of 1 cm path length and reported as TAA (turbidimetry on apparent absorbance). The solution temperature was increased from 10 to 90 °C with 2 °C every 5 min then decreased back to 10 °C, monitoring the absorbance under stirring after 5 min to reach the temperature equilibrium.

Thioflavin T (ThT) fluorescence assay

The assay for binding of thioflavin-T was performed according to the method of LeVine.[57] ThT fluorescence emission was measured with excitation at 440 nm between 460 and 500 nm with 5 nm slit widths using a JOBIN YVON-SPEX FUOROLOG-3 spectrofluorometer. A stock solution of 2.5 mM Thioflavin T (ThT) was prepared in TBS buffer and filtered by a 0.22 μm filter. 1 ml ThT stock solution was added to 50 ml TBS to a final concentration of 50 μM. Fluorescence spectra in the presence of peptides recovered from turbidimetry were measured. The spectrum of peptide alone was subtracted from the spectrum of the ThT solution with peptide to normalise the fluorescence of the sample by subtracting the blank sample.

Congo red spectral shift assay

The procedure described by Klunk *et al.*[31] was followed, with minor modifications. A Congo red stock solution (1.25 mM) was prepared in TBS buffer–ethanol (8 : 2, v/v) at pH 7.4 and filtered by using a 0.22 μm filter. From this stock solution, a diluted Congo red solution was prepared (0.125 mM). Aliquots (0.350 ml) taken from peptide suspensions recovered from turbidimetry experiment in TBS were combined with 0.350 ml of the Congo red solution (0.125 mM). The peptide suspensions were stirred, and an absorbance spectrum from 400 to 600 nm was collected with a NIR-UV O5 Cary UV spectrophotometer using quartz cells of 1 cm path length and TBS as reference solution. The spectrum of peptide alone was subtracted from the spectrum of Congo Red with peptide to correct for the turbidity of the sample due to the precipitated material.

Congo red birefringence assay

50 μl of each polypeptide solution previously analysed by Congo red binding assay, were deposited onto a glass slide and air-dried at room temperature. The slides were observed at 40X magnification. The stained samples were examined under polarised light with a Nikon ECLIPSE E600 POL microscope equipped with Nikon Cool Pix 4500 4.0 Mega Pixel.

FTIR spectroscopy

The synthesised peptides were analysed by FTIR in KBr pellets (1 mg 100 mg^{-1}) as a powder. S4 peptide was also analysed as precipitated fibres. The spectra were recorded on a Jasco FTIR-460 PLUS using a resolution of 2 cm^{-1} and and 256 scan, then smoothed by using the Savitzky–Golay algorithm. S3 and S4 peptides were analysed in D_2O solution (5 mg ml^{-1}) by using CaF_2 cells of 200 micron path length. The decomposition of FTIR spectra was obtained using the peak fitting module implemented in the Origin Software (Microcalc Inc.) using the second derivative method. In the curve fitting procedure, the Voigt peak shape has been used for all peaks. The Voigt shape is a combination of the Gaussian and Lorentzian peak shapes and accounts for the broadening present in the FTIR spectrum.

MD simulations

MD simulations were focused on the S3 and S4 peptides as they are the two longest peptides. The simulations were performed in water (explicit solvent) and in boxes with the following dimensions 35 × 35 × 90 Å^3. The simulations refer to single molecule and its conformational changes. All the calculations were performed on the regional computing platform ROMEO2 (http://www.romeo2.fr/), constituted of 11 nodes for a total of 108 cores (400 GB RAM). Processors are dual-core Intel Itanium II (Montecito) possessing 8 MB cache with a 1.6 GHz frequency. The cluster of the Multi-scale Molecular Modelling Platform was also used (2 × 8 cluster vision CPU).The simulations are 100 ns long. Each peptide was generated using the RIBOSOME V1.0 program (http://rose-lab.jhu.edu/~raj/Manuals/ribosome.html). Two starting conformations were generated for the two peptides; both elongated and PPII structures were considered as the starting point. Each of these structures are characterised by specific values of the torsions angles of the residues along the sequence: the canonical ($\varphi = -180°$; $\psi = +180°$) values were used in the case of the elongated starting configuration whereas the canonical ($\varphi = -75°$; $\psi = +145°$) values were used in the case of the PPII starting structure. First, the peptides were placed in TIP3 water box.[62] The extended conformation of S4 in water contains 10 859 atoms and 3533 water molecules. Concerning S3, while the number of atoms per box is very similar to S4, the number of solvent molecules is higher as the

peptide is shorter than S4. We did not perform replicate runs. Periodic boundary conditions were applied during all stages of the simulation. The water molar ratio was not taken into account in the simulations. Since we have run single peptide simulations, the size of the box was chosen so that the peptide would not interact with its images when we apply the periodic boundary conditions. The entire solute–solvent system was minimised, by applying 500 steps of energy minimisation using the steepest descent algorithm. The system was then heated to 310 K and molecular dynamics simulations were performed using the GROMACS software Version 4.0.7, using the OPLSAA[63] force-field, on a supercomputer of the ROMEO2 platform. The Verlet algorithm was used to integrate the equations from classical mechanics, in parallel with an integration step of 2 fs since we froze the length of the bonds implicating hydrogen atoms. For the nonbonded terms, we used the Particle Mesh Ewald (PME) algorithm with a cut off at 1.49 Å for the coulombic interactions and a potential-shifting function for van der Waals interactions applied at 1.3 Å and a cut off at 1.4 Å.

Atomic Force Microscopy (AFM)

At the end of the warming cycle of turbidity assay, the suspension was centrifuged and the supernatant was removed. The pellet was washed with ultra-pure water, centrifuged and the supernatant removed. The process was repeated twice in order to remove salts. 10 microliters of the suspension was deposited on Silicon (100) wafer substrate (Aldrich, Saint Louis, Mo, USA) and on Mica squares, 0,15 mm thickness, size 15 mm × 15 mm (NT-MDT America Inc. Santa Clara, CA 95054, USA). The silicon wafers were cleaned by using a two-solvent method consisting in the immersion of the Si wafer in warm acetone bath for a period of 10 min. Then a methanol bath for a period of 5 min immediately followed with final deionized water rinses. The samples were air-dried and repeatedly rinsed with ultra-pure water in order to remove salts. After water evaporation, the AFM images were carried out by using the XE-120 microscope (Park Systems) in air and at room temperature. Data acquisition was carried out in intermittent contact mode at scan rates between 0.4 and 3 Hz, using rectangular Si cantilevers (NCHR, Park Systems) having the radius of curvature less than 10 nm and with the nominal resonance frequency and force constant of 330 kHz and 42 N m^{-1}, respectively, or diamond tips (Mikromasch) with typical spike curvature radius less than 7 nm, nominal resonance frequency of 325 kHz, and typical force constant 46 N m^{-1}.

Acknowledgements

The financial support from the Italian Ministry of University and Research (MIUR) (PRIN 2010-Project 2010L(SH3K) to B.B.) is gratefully acknowledged. The authors thank the HPC – Regional Center ROMEO and the Multiscale Molecular Modeling Platform (P3M) from the University of Reims Champagne Ardenne (France) for providing CPU time and support. Thanks are due to Dr Neluta Ibris for AFM images (CIGAS-University of Basilicata). We thank Prof. Ivonne Pasquali-Ronchetti (University of Modena-Reggio Emilia) for critical reading of the manuscript.

References

1 A. M. Tamburro, *Nanomedicine*, 2009, **4**, 469–487.
2 M. A. Gibson, G. Hatzinikolas, J. S. Kumaratilake, L. B. Sandberg, J. K. Nicholl, G. R. Sutherland and E. G. Cleary, *J. Biol. Chem.*, 1996, **271**, 1096–1103.
3 S. G. Wise and A. S. Weiss, *Int. J. Biochem. Cell Biol.*, 2009, **41**, 494–497.
4 J. E. Wagenseil and R. P. Mecham, *J. Cardiovasc. Transl. Res.*, 2012, **5**, 264–273.
5 C. M. Kielty, *Expert Rev. Mol. Med.*, 2006, **8**, 1–23.
6 F. Antonicelli, G. Bellon, L. Debelle and W. Hornebeck, *Curr. Top. Dev. Biol.*, 2007, **79**, 99–155.
7 J. S. Campa, R. M. Greenhalgh and J. T. Powell, *Atherosclerosis*, 1987, **65**, 13–21.
8 G. M. Longo, S. J. Buda, N. Fiotta, W. Xiong, T. Griener, S. Shapiro and B. T. Baxter, *Surgery*, 2005, **137**, 457–462.
9 S. Matsumoto, T. Kobayashi, M. Katoh, S. Saito, Y. Ikeda, M. Kobori, Y. Masuho and T. Watanabe, *Am. J. Pathol.*, 1998, **153**, 109–119.
10 J. H. Chung, J. Y. Seo, M. K. Lee, H. C. Eun, J. H. Lee, S. Kang, G. J. Fisher and J. J. Voorhees, *J. Invest. Dermatol.*, 2002, **119**, 507–512.
11 D. P. Varadi, *J. Invest. Dermatol.*, 1972, **59**, 238–246.
12 K. Fan and W. A. Nagle, *BMC Pulm. Med.*, 2002, **2**, 5.
13 S. Doostkam, J. R. Bohl, A. Sahraian and A. A. Mahjoor, *Pak. J. Biol. Sci.*, 2008, **11**, 1852–1855.
14 B. Bochicchio, A. Pepe, R. Flamia, M. Lorusso and A. M. Tamburro, *Biomacromolecules*, 2007, **8**, 3478–3486.
15 A. M. Tamburro, A. Pepe, B. Bochicchio, D. Quaglino and I. P. Ronchetti, *J. Biol. Chem.*, 2005, **280**, 2682–2690.
16 A. M. Tamburro, M. Lorusso, N. Ibris, A. Pepe and B. Bochicchio, *Chirality*, 2010, **22**, E56–66.
17 S. Taddese, A. S. Weiss, R. H. Neubert and C. E. Schmelzer, *Matrix Biol.*, 2008, **27**, 420–428.
18 A. F. Drake, G. Siligardi and W. A. Gibbons, *Biophys. Chem.*, 1988, **31**, 143–146.
19 R. W. Woody, *Adv. Biophys. Chem.*, 1992, **2**, 37–79.
20 Z. Shi, R. W. Woody and N. R. Kallenbach, *Adv. Protein Chem.*, 2002, **62**, 163–240.
21 Z. Shi, C. A. Olson, G. D. Rose, R. L. Baldwin and N. R. Kallenbach, *Proc. Natl. Acad. Sci. U. S. A.*, 2002, **99**, 9190–9195.
22 B. Bochicchio and A. M. Tamburro, *Chirality*, 2002, **14**, 782–792.
23 B. Bochicchio, A. Ait-Ali, A. M. Tamburro and A. J. Alix, *Biopolymers*, 2004, **73**, 484–493.
24 B. Bochicchio, N. Floquet, A. Pepe, A. J. Alix and A. M. Tamburro, *Chem.–Eur. J.*, 2004, **10**, 3166–3176.
25 A. M. Tamburro, B. Bochicchio and A. Pepe, *Biochemistry*, 2003, **42**, 13347–13362.
26 D. S. Wishart, B. D. Sykes and F. M. Richards, *Biochemistry*, 1992, **31**, 1647–1651.
27 P. F. Fuchs, A. M. Bonvin, B. Bochicchio, A. Pepe, A. J. Alix and A. M. Tamburro, *Biophys. J.*, 2006, **90**, 2745–2759.
28 K. M. Fiebig, H. Schwalbe, M. Buck, L. J. Smith and C. M. Dobson, *J. Phys. Chem.*, 1996, **100**, 2661–2666.

29 G. J. Sharman and M. S. Searle, *J. Am. Chem. Soc.*, 1998, **120**, 5291–5300.
30 C. Camilloni, A. De Simone, W. F. Vranken and M. Vendruscolo, *Biochemistry*, 2012, **51**, 2224–2231.
31 W. E. Klunk, R. F. Jacob and R. P. Mason, *Methods Enzymol.*, 1999, **309**, 285–305.
32 A. A. Maskevich, V. I. Stsiapura, V. A. Kuzmitsky, I. M. Kuznetsova, O. I. Povarova, V. N. Uversky and K. K. Turoverov, *J. Proteome Res.*, 2007, **6**, 1392–1401.
33 S. P. Graether, R. Kisilevsky and R. Young ID, *Amyloid Int. J Exp. Clin. Invest.*, 1996, **3**, 20–27.
34 R. A. DeLellis, G. G. Glenner and J. S. Ram, *J. Histochem. Cytochem.*, 1968, **16**, 663–665.
35 P. Ladewig, *Nature*, 1945, **156**, 81–82.
36 S. Krimm, *J. Mol. Biol.*, 1962, **4**, 528–540.
37 T. B. Miyazawa and E. R. Blout, *J. Am. Chem. Soc.*, 1961, **83**, 712–719.
38 S. Cai and B. R. Singh, *Biochemistry*, 2004, **43**, 2541–2549.
39 M. M. Jackson and H. H. Mantsch, *Biochim. Biophys. Acta, Protein Struct. Mol. Enzymol.*, 1991, **1078**, 231–235.
40 A. M. Tamburro, S. Panariello, V. Santopietro, A. Bracalello, B. Bochicchio and A. Pepe, *ChemBioChem*, 2010, **11**, 83–93.
41 W. K. Surewicz, H. H. Mantsch and D. Chapman, *Biochemistry*, 1993, **32**, 389–394.
42 J. C. Andries, J. M. Anderson and A. G. Walton, *Biopolymers*, 1971, **10**, 1049–1057.
43 J. Bandekar, *Biochim. Biophys. Acta, Protein Struct. Mol. Enzymol.*, 1992, **1120**, 123–143.
44 M. R. Nilsson, *Methods*, 2004, **34**, 151–160.
45 F. Eker, K. Griebenow and R. Schweitzer-Stenner, *Biochemistry*, 2004, **43**, 6893–6898.
46 J. Jarvet, P. Damberg, J. Danielsson, I. Johansson, L. E. Eriksson and A. Graslund, *FEBS Lett.*, 2003, **555**, 371–374.
47 R. Tycko, *Curr. Opin. Struct. Biol.*, 2004, **14**, 96–103.
48 A. Pepe, M. R. Armenante, B. Bochicchio and A. M. Tamburro, *Soft Matter*, 2009, **5**, 104–113.
49 K. F. DuBay, A. P. Pawar, F. Chiti, J. Zurdo, C. M. Dobson and M. Vendruscolo, *J. Mol. Biol.*, 2004, **341**, 1317–1326.
50 B. Bochicchio, A. Pepe and A. M. Tamburro, *Future Neurol.*, 2007, **2**, 523–536.
51 A. Pepe, D. Guerra, B. Bochicchio, D. Quaglino, D. Gheduzzi, I. Pasquali Ronchetti and A. M. Tamburro, *Matrix Biol.*, 2005, **24**, 96–109.
52 G. C. Yeo, F. W. Keeley and A. S. Weiss, *Adv. Colloid Interface Sci.*, 2011, **167**, 94–103.
53 B. Bochicchio and A. Pepe, *Chirality*, 2011, **23**, 694–702.
54 L. D. Muiznieks and F. W. Keeley, *J. Biol. Chem.*, 2010, **285**, 39779–39789.
55 S. Rauscher, S. Baud, M. Miao, F. W. Keeley and R. Pomes, *Structure*, 2006, **14**, 1667–1676.
56 M. Lorusso, A. Pepe, N. Ibris and B. Bochicchio, *Soft Matter*, 2011, **7**, 6327–6336.
57 M. Gasset, M. A. Baldwin, D. H. Lloyd, J. M. Gabriel, D. M. Holtzman, F. Cohen, R. Fletterick and S. B. Prusiner, *Proc. Natl. Acad. Sci. U. S. A.*, 1992, **89**, 10940–10944.
58 K. Tamiola, B. Acar and F. A. Mulder, *J. Am. Chem. Soc.*, 2010, **132**, 18000–18003.
59 A. W. Bryan, Jr., M. Menke, L. J. Cowen, S. L. Lindquist and B. Berger, *PLoS Comput. Biol.*, 2009, **5**, e1000333.
60 A. M. Fernandez-Escamilla, F. Rousseau, J. Schymkowitz and L. Serrano, *Nat. Biotechnol.*, 2004, **22**, 1302–1306.
61 K. K. Frousios, V. A. Iconomidou, C. M. Karletidi and S. J. Hamodrakas, *BMC Struct. Biol.*, 2009, **9**, 44.
62 S. O. Garbuzynskiy, M. Y. Lobanov and O. V. Galzitskaya, *Bioinformatics*, 2010, **26**, 326–332.
63 O. Conchillo-Sole, N. S. de Groot, F. X. Aviles, J. Vendrell, X. Daura and S. Ventura, *BMC Bioinformatics*, 2007, **8**, 65.
64 S. Maurer-Stroh, M. Debulpaep, N. Kuemmerer, M. Lopez de la Paz, I. C. Martins, J. Reumers, K. L. Morris, A. Copland, L. Serpell, L. Serrano, J. W. Schymkowitz and F. Rousseau, *Nat. Methods*, 2010, **7**, 237–242.
65 G. G. Tartaglia and M. Vendruscolo, *Chem. Soc. Rev.*, 2008, **37**, 1395–1401.
66 S. J. Hamodrakas, *FEBS J.*, 2011, **278**, 2428–2435.
67 B. Haggqvist, J. Naslund, K. Sletten, G. T. Westermark, G. Mucchiano, L. O. Tjernberg, C. Nordstedt, U. Engstrom and P. Westermark, *Proc. Natl. Acad. Sci. U. S. A.*, 1999, **96**, 8669–8674.
68 S. Peng, A. Larsson, E. Wassberg, P. Gerwins, S. Thelin, X. Fu and P. Westermark, *Lab. Invest.*, 2007, **87**, 1195–1205.